

## Birefringent pipes: the steady flow of a dilute polymer solution near a stagnation point

O.G. Harlen, E.J. Hinch and J.M. Rallison

*Department of Applied Mathematics and Theoretical Physics, University of Cambridge, Cambridge CB3 9EW (UK)*

(Received October 24, 1991; in revised form January 13, 1992)

### Abstract

In steady flows at high Deborah numbers high polymer stresses are often concentrated within thin boundary layers along streamlines downstream of flow stagnation points where the polymer extension is large. The layers appear as birefringent lines in optical experiments.

Detailed observations of the flow near a stagnation point have shown a complex sequence of birefringence structures, which appear as the flow rate increases, for polymer concentrations above some critical value. The first transition is from a solid birefringent line to a hollow birefringent cylinder or 'pipe'. In this paper we calculate the modification of the flow due to the presence of polymer for a FENE (finitely extensible non-linear elastic) dumbbell model with non-linear hydrodynamic friction, and demonstrate that the associated reduction in strain rate at the stagnation point can be sufficient to produce a pipe structure. The polymer concentrations required to produce this transition are found to be in qualitative agreement with experiment.

We determine also the thickness of birefringent strands as a function of polymer concentration, molecular weight, flow rate and inertia. These results too are found to be in qualitative agreement with experiment.

We show finally that for a FENE model with constant hydrodynamic friction birefringent strands are produced, but we do not find pipes at realistic values of the parameters.

*Keywords:* birefringent pipes; coil-stretch hysteresis; dumbbell model; elongational flow; FENE model; high Deborah number; polymer solution; stagnation point

---

*Correspondence to:* J.M. Rallison, Department of Applied Mathematics and Theoretical Physics, University of Cambridge, Cambridge CB3 9EW, UK.

## 1. Introduction

Even at dilute concentrations ( $c < c^*$ ) the presence of polymers can produce a large increase in the extensional viscosity of a solution [1]. At low Deborah numbers the polymer molecules adopt a randomly coiled configuration and at dilute concentrations produce only a small change in the viscosity of the solution. However, in steady extension at high Deborah numbers the polymer molecules can become highly extended by the flow, so that the effective volume fraction occupied by the polymer (which is given by the largest linear dimension of the molecule) becomes much larger. The polymer solution then behaves like a semidilute suspension of rods and has a greatly enhanced extensional viscosity [2].

Two criteria must be met for high polymer extension to take place in a flow. First, the extension rate of the flow must be sufficiently large to overcome the relaxation of the polymer (i.e. the Deborah number must exceed unity). Second, the polymer must remain within the region of extensional flow for sufficient time to experience a large strain. In a steady flow, this latter condition is met, in general, only by those molecules which pass close to a stagnation point. As a result, highly extended polymers are confined to narrow regions at, and downstream of, stagnation points. In optical birefringence experiments (e.g. ref. [3]), these regions of high polymer extension appear as bright birefringent lines and hence we called them 'birefringent strands' in an earlier paper [4]. This structure is also seen in the high Deborah number computations of Chilcott and Rallison [5].

In two previous papers [4,6] we constructed an asymptotic method to analyse steady high-Deborah-number flows with stagnation points. The birefringent strands are regarded as force singularities within an otherwise Newtonian fluid and the consequent modification of the flow outside the strands is calculated. For planar flows only one parameter  $\lambda$  is needed to characterise this non-Newtonian flow modification, namely the product of the width of the strand and its high extensional viscosity. An analogous quantity  $\hat{\lambda}$  may be defined for axisymmetric flows. Although these results came from a study using a FENE dumbbell model, we have noted also [6] that any constitutive model (e.g. Phan–Thien–Tanner or Giesekus) exhibiting a high, but finite, Trouton ratio may be expected to give qualitatively similar results for the flow modification outside the strands.

In this paper we consider the structure of the birefringent strand itself and attempt to calculate the parameter  $\lambda$  as a function of the polymer concentration, molecular weight and the extension rate of the flow for a FENE model. For small values of  $\lambda$  this task is straightforward: the flow is approximately Newtonian everywhere and  $\lambda$  can then be determined by a

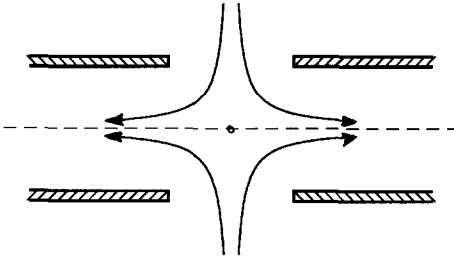


Fig. 1. Sketch of the opposed-jet device.

purely kinematic calculation [4,6,7]. At higher values of  $\lambda$ , however, the presence of the highly viscous fluid within the strand reduces the extension rate in the neighbourhood of the strand, and a self-consistent calculation of the flow modification is needed. Different constitutive models may not give similar results here. We choose to focus on a FENE model.

In circumstances where flow modification occurs, birefringence experiments suggest that the form of the modification may be complex. In a series of experiments with several different monodisperse polymer solutions Keller, Odell and co-workers [8–13] and also Cathey and Fuller [14] have carefully studied the flow birefringence near an axisymmetric stagnation point using an opposed-jet device (see Fig. 1). Polymer solution is sucked simultaneously through both jets, creating a stagnation point at the centre point between the jets. An extension rate may be defined from the overall volumetric flow rate.

At very low concentrations a thin birefringent strand is observed for all extension rates above the coil–stretch transition value but no flow modification is seen. At higher concentrations (though still at concentrations below the critical concentration for entanglements between neighbouring coiled molecules,  $c^*$ ) a more complex behaviour is found. Above a critical extension rate a thin birefringent strand appears. As the extension rate is increased, the region of birefringence becomes much broader and above a second critical extension rate a dark central line appears within the birefringent strand. This structure, in which the region of birefringence has a non-birefringent interior, is termed a *pipe*. Upon further increases in extension rate the dark interior widens and a second and occasionally even a third birefringent line may appear along the centre line. Ultimately the flow becomes unstable and rapidly fluctuating birefringence appears throughout the flow. This unstable state is termed the *flare*.

A similar sequence is observed for planar flows by Cressely et al. [15,16] in two-roll mills. As the roller speed is increased, a thin birefringent line appears, this line then broadens before appearing to split into two. At still higher speeds the flow becomes unstable.

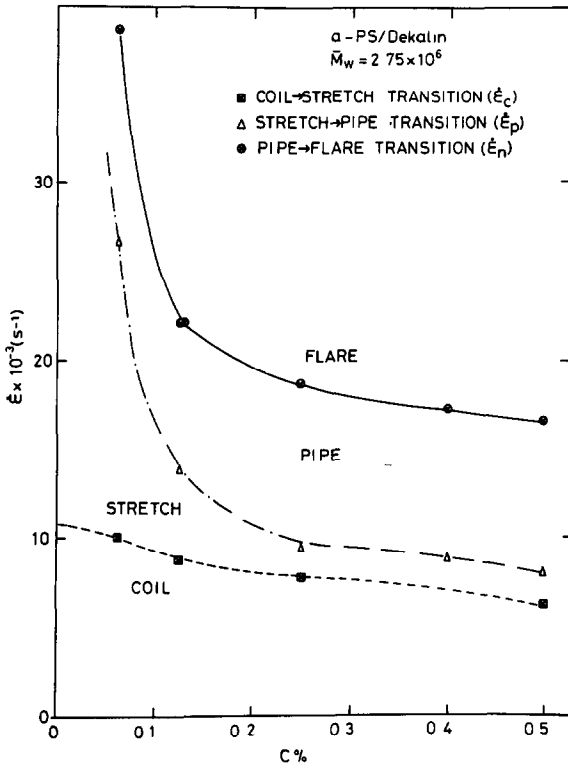


Fig. 2. Phase diagram of the birefringence behaviour of solutions of monodisperse polystyrene (taken from Keller et al. [9]).

Figure 2 (taken from Keller et al. [9]) shows a 'phase diagram' of the birefringence behaviour as a function of extension rate and polymer concentration for solutions of monodisperse polystyrene. Pipes do not occur at concentrations below a critical value,  $c_+$ . For  $c > c_+$  pipes appear only at extension rates above a second critical extension rate (which depends strongly on  $c$  and is higher than the coil–stretch value).

The structure of the birefringence in the pipe suggests (on the assumption that birefringence and high extension are equivalent) that polymer molecules are extended only in the outer part of the strand where the flow is birefringent and not in the interior where there is no birefringence. Thus, polymer molecules which were highly extended in the outer part of the strand appear to collapse back towards the coiled state as they enter the dark interior region. As noted by Keller et al. [9], this can occur only if the strain rate within the interior is lower than the critical strain rate at which extended polymers collapse (the stretch–coil transition). Outside the

strand the strain rate is above the coil–stretch value and so there must be a large decrease in strain rate within the strand. Velocity measurements by Gardner et al. [17] in a cross-slot device do indeed show a sharp decrease in extension rate at the position of the strand.

Keller et al. suggests that this reduction in the strain rate arises from entanglements between polymer molecules, even though pipes occur at concentrations much smaller than  $c^*$ . The presence of a critical concentration for pipe formation would appear to support this theory. We suggest, however, that pipes can occur at dilute polymer concentrations without direct mechanical interactions between neighbouring molecules (i.e. no entanglements). We do, of course, include interactions mediated by the solvent which are vital to the cooperative effect.

To test this hypothesis we construct a self-consistent model of the flow field near a stagnation point. An essential feature of this model is that it includes the modification of the flow due to the presence of the extended polymers. In order to obtain the correct behaviour for the stretch–coil transition, we use a dumbbell model incorporating non-linear friction [18] to model the polymer. Using this model we are able to produce not only birefringent pipes, but also a phase diagram similar to Fig. 2. Perhaps surprisingly, we find also that without including a non-linear friction term we cannot produce the pipe behaviour at plausible parameter values. It remains to be determined whether other constitutive models can produce birefringent pipes.

In most of the experiments performed by Keller's group, low-viscosity solvents are used and consequently the Reynolds numbers are quite large (of the order of 100 in the experiments of Müller et al. [11]), despite the small scale of their apparatus. However, in more recent experiments [13,19], and in those of Cathey and Fuller [14], more viscous solvents are used for which the Reynolds numbers are less than one. Qualitatively, the phase diagram (Fig. 2) is found to be insensitive to Reynolds number. For a first analysis we choose to neglect inertia in our model. However, inertia does appear to affect the width of the birefringent strand at high strain rates and this is discussed separately in Section 6.

## 2. A model problem

In order to investigate the effects of flow modification on the structure of the birefringent strand, we construct a model of the steady flow in the neighbourhood of the strand. This model is necessarily highly simplified, but does contain the physical mechanisms which we believe are important in determining the qualitative features of the flow.

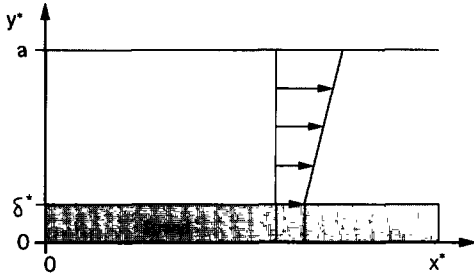


Fig. 3. Sketch of flow geometry.

## 2.1 Flow geometry

There are two difficulties in providing a detailed analysis of the flows in the opposed-jet and cross-slot experiments. First, the velocity field and extent of the polymer deformation upstream of the stagnation point are poorly characterised; in consequence we shall employ upstream boundary conditions that are as simple as possible. Second, the flow near, but downstream of, the stagnation point is fully two-dimensional. We show below that, by means of a suitable choice for the external flow, lubrication methods can be used to simplify this calculation. More complex numerical solutions will be required to remedy these defects to provide a full solution for the cross-slot flow.

### 2.1.1 Planar flow

For two-dimensional flow near a stagnation point, we employ Cartesian coordinates  $(x^*, y^*)$  with the origin at the stagnation point and the direction of extension parallel to the  $x^*$ -axis (see Fig. 3). We assume that the polymers are extended only within a distance  $a$  of the  $x^*$ -axis, and we construct a model of the flow within a semi-infinite strip of width  $a$ , with some prescribed flow on the boundary  $y^* = a$ .

The tangential velocity on the boundary  $y^* = a$  is determined by the external flow, and so we require that the  $x^*$ -component of the velocity,  $u^*$ , be equal to some prescribed function  $\mathcal{U}^*(x^*)$  on  $y^* = a$ . In choosing a suitable form for  $\mathcal{U}^*(x^*)$  we note that near the stagnation point  $\mathcal{U}^*$  is proportional to  $x^*$  but, as the region of extensional flow is finite in length, we require  $\mathcal{U}^*$  to tend to a finite limit at large distances. As a model problem we take

$$\mathcal{U}^*(x^*) = U_\infty [1 - \exp(-x^*/b)], \quad (1)$$

where  $b$  is the length scale in the  $x^*$  direction.

In analysing the cross-slot flow the most appropriate choice would perhaps be  $b = a$ , so that the prescribed flow would be small on the walls of the downstream tube ( $y^* = a, x^* > a$ ). As indicated above, to make the calculation tractable we shall, however, assume that  $b \gg a$  so that the flow is almost unidirectional almost everywhere and lubrication methods can be employed.

Additionally we take as a second convenient boundary condition that the normal force on the wall  $y = a$  vanishes. It follows that the pressure gradient associated with the flow vanishes at leading order in  $a/b$  and thus outside the birefringent strand itself the velocity profile is linear in  $y$ . The normal component of velocity on  $y = a$  will be determined from continuity, and will be necessarily small, but non-zero.

The remaining boundary conditions on  $u^*$  are that  $u^* \rightarrow U_\infty$  as  $x^* \rightarrow \infty$  and (from symmetry) that

$$u^* |_{x^*=0} = 0 \quad \text{and} \quad \left. \frac{\partial u^*}{\partial y^*} \right|_{y^*=0} = 0. \tag{2}$$

### 2.1.2 Axisymmetric flow

For uniaxial extension, we can form the analogous model to that of Section (2.1.1) for a cylindrical geometry. We use cylindrical polar coordinates  $(r^*, z^*)$  with the origin at the stagnation point and the  $z^*$ -axis along the centre line of the strand. As before, we calculate the fluid velocity  $u = (v^*, w^*)$  within a semi-infinite cylinder of radius  $a$  for an imposed velocity  $w^* = \mathcal{U}^*(z^*) = U_\infty[1 - \exp(-z^*/b)]$  at  $r = a$ . Again we suppose that  $b \gg a$ , and that no pressure gradient is exerted.

### 2.1.3 Non-dimensionalisation

It is convenient to rescale dimensions so that in planar flow

$$x = \frac{x^*}{b}, \quad y = \frac{y^*}{a}, \quad u = \frac{u^*}{U_\infty}, \quad v = \frac{v^*b}{U_\infty a} \tag{3}$$

and in axisymmetric flow

$$z = \frac{z^*}{b}, \quad r = \frac{r^*}{a}, \quad w = \frac{w^*}{U_\infty}, \quad v = \frac{v^*b}{U_\infty a}. \tag{4}$$

## 2.2 Polymer model

The distortion of the polymer is modelled as the extension of an elastic dumbbell that incorporates both a non-linear spring and non-linear friction

[18]. In the flow geometry described in Section 2.1 the extension of the dumbbells is predominantly in the direction parallel to the  $x$ -axis, and so we shall only consider the extension of dumbbells in this direction. The evolution of the dimensionless dumbbell extension,  $R$ , is given by

$$\frac{dR}{dt} = R \frac{\partial u}{\partial x} - \frac{4f(R)}{DR} (R - 1). \quad (5)$$

where  $d/dt$  is a Lagrangian time derivative,  $D$  is the Deborah number, scaled so that the critical extension rate required to extend the dumbbells corresponds to a Deborah number of unity, and  $f(R)$  is given by

$$f(R) = \frac{1}{1 - (R^2/L^2)},$$

where  $L$  is the extensibility of the dumbbells, and we shall assume that  $L \gg 1$ .

The elastic stress is predominantly in the  $\hat{x}\hat{x}$ -direction, and has magnitude,  $\sigma_p$  where [7]

$$\sigma_p = \frac{4\mu c}{D} f(R) R^2. \quad (6)$$

While this model is an oversimplification it has the correct asymptotic features for a strong extensional flow. First, the length of a dumbbell tends to a finite limit  $L$  at high extension rates. Second, when fully extended the dumbbells behave like rigid rods, giving a viscous stress proportional to the extension rate, with an extensional viscosity

$$\mu_p \approx \frac{1}{2} \mu c L^3. \quad (7)$$

There is also a hysteresis [18] between the coil–stretch and stretch–coil transitions, because the strain rate required to maintain the extension of a highly extended dumbbell is lower than that required to stretch an unextended dumbbell (see Fig. 4).

## 2.3 Calculation of the flow

### 2.3.1 The two-fluid approximation

A full calculation of the flow near a stagnation point requires a numerical solution of coupled partial differential equations for the fluid velocity and the polymeric stress (determined from the extension of the dumbbells). In view of the high stress gradients within the strand and the disparity of length scales (with a strand width small compared to  $a$ , but a strand length large compared to  $a$ ) such a numerical calculation would be difficult. (In

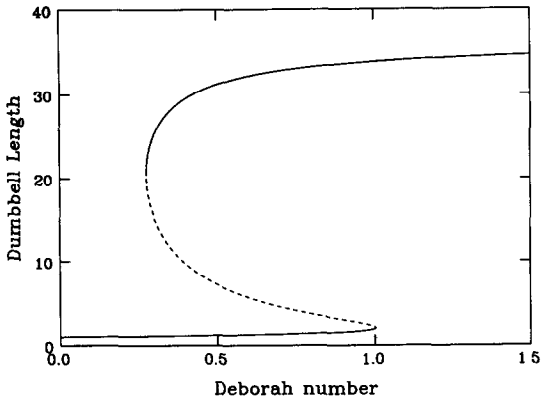


Fig. 4. Graph of the equilibrium dumbbell lengths in steady extensional flow for  $L = 36$ . Solid lines indicate stable solutions; dotted lines unstable solutions. Note the existence of multiple stable solutions in the range 0.3 to 1.0.

simulations with a simpler FENE dumbbell model Chilcott and Rallison [5] were restricted to values of  $L$  of at most 10.) Fortunately for large values of  $L$  the system may be decoupled by means of a two-fluid approximation [7,20]. The flow is divided into two distinct regions.

(1) Outside the strand, the extension of the polymers is not sufficient to produce high non-Newtonian stresses and so the dominant contribution to the stress comes from solvent. The fluid, therefore, behaves as a Newtonian fluid of approximately solvent viscosity ( $\mu$ ).

(2) Within the strand the polymers are highly extended and aligned in the direction of extension. The extended polymers behave like rigid rods and so the solution behaves as an anisotropic viscous fluid with a greatly enhanced extensional viscosity ( $\mu_p$ ).

### 2.3.2 The incoming stagnation streamline

Instead of solving eqn. (5) for the stretch of the polymer molecule along all the streamlines, we calculate the stretch only along one representative streamline, the incoming stagnation streamline. We show in the Appendix that while the strand is thin compared with the channel width, the stretch of the polymers near to the strand depends only on  $y$ , and so is identical to that on the incoming stagnation streamline. Substantial flow modification can be generated by a thin strand, but not enough to produce a pipe. Thus we find that pipes occur only when the strand occupies a significant fraction of the channel. Unfortunately, we are unable to prove that the stretch is independent of  $x$  in this case. Experiments do, however, find that the birefringence is quite uniform along the strand, and we shall assume that the strand width remains uniform in the analysis that follows.

Along the incoming stagnation streamline, eqn. (5) becomes

$$v \frac{\partial R}{\partial y} = -R \frac{\partial v}{\partial y} - \frac{4f(R)}{RD} (R-1), \quad (8)$$

with the initial condition that  $R = 1$  at  $y = 1$ . The strand width  $\delta$  is then given as the value of  $y$  at which  $R$  becomes nearly equal to  $L$ . In our simplified numerical calculations we choose to define the outside edge of the strand,  $y = \delta$ , to be at the point of the maximum extension, i.e. where  $\partial R / \partial y = 0$ .

### 2.3.3 Thin strands and thick strands

For values of the parameters  $c (\ll 1)$ ,  $L (\gg 1)$  and  $D$  for which  $\delta$  proves to be small and the variation in the fluid velocity across the strand is small, analytic progress is possible. For a thin strand the jump in the tangential stress  $(\mu U/a) \partial u / \partial y$  across the strand is balanced by the divergence of the extensional stress within the strand [4] and so, given that the polymers are fully stretched in this region

$$\left. \frac{\partial u}{\partial y} \right|_{y=\delta} = - \frac{\partial}{\partial x} \left( \Lambda \frac{\partial u}{\partial x} \right), \quad (9)$$

where the non-Newtonian parameter  $\Lambda$  is equal to

$$\Lambda = \frac{2\mu_p \delta a^2}{\mu b^2}. \quad (10)$$

For our chosen polymer model,  $\mu_p = \frac{1}{2} \mu c L^3$ . We find that the polymer concentration  $c$  only occurs in the combination

$$\hat{c} = ca^2/b^2 \quad (11)$$

and with this definition

$$\Lambda = \hat{c} L^3 \delta, \quad (12)$$

so that the non-Newtonian parameter  $\lambda$  used in ref. 4 is given as  $\lambda = \Lambda b^2/a$ .

In Section 3 we show by means of an analytical argument that there is a strong suggestion that a pipe will occur for suitably large values of  $\Lambda$ , but within the thin strand limit we are unable to predict the details of the flow within the pipe once it has formed.

The case where the variation of the fluid velocity within the strand is significant requires a calculation of the flow both inside and outside the strand and, even with the two-fluid approximation, a numerical solution is needed (see Section 4). Note that in these numerical solutions we are

forced to assume that the stretch of the polymer, and hence  $\delta$  and  $\Lambda$ , are constant along the strand.

### 3. Thin strands

#### 3.1 Planar flow

Outside the strand the fluid is Newtonian and so with the lubrication approximation the fluid velocity satisfies

$$\frac{\partial^2 u}{\partial y^2} = 0 \quad \delta < y \leq 1. \tag{13}$$

Hence if  $U(x)$  is the velocity within the strand (variations across the strand being supposed negligible) we have

$$u(x, y) = \begin{cases} U(x) & 0 \leq y \leq \delta, \\ U(x) + (y - \delta)(\mathcal{U} - U) & \delta \leq y \leq 1; \end{cases} \tag{14}$$

on continuity grounds  $v$  is then given by

$$v(x, y) = -U'y - \frac{1}{2}(y - \delta)^2(U' - \mathcal{U}') \quad \delta \leq y \leq 1. \tag{15}$$

The jump in  $\partial u/\partial y$  across the strand is given by eqn. (9) and so

$$\Lambda U'' - U = -\mathcal{U}. \tag{16}$$

The solution of this equation satisfying the boundary conditions (2) is

$$U = 1 + \frac{1}{\Lambda - 1} \exp(-x) - \frac{\Lambda}{\Lambda - 1} \exp\left(-\frac{x}{\Lambda^{1/2}}\right), \tag{17}$$

and hence the strain rate at the origin,  $U'$ , and the velocity,  $v$ , along the incoming stagnation streamline are given as

$$U' = \frac{1}{1 + \Lambda^{1/2}}, \quad v = -\frac{1}{1 + \Lambda^{1/2}}y - \frac{\Lambda^{1/2}}{2(1 + \Lambda^{1/2})}y^2. \tag{18}$$

This solution can be valid only if variations in the strain rate  $\partial u/\partial x (= -\partial v/\partial y)$  are negligible in the region  $y < \delta$ , and thus for consistency we require that  $\Lambda^{1/2}\delta \ll 1$ .

We assume that  $D$  is sufficiently large that polymers become stretched, and then eqn. (8) may be used to estimate the degree of stretch of the polymers as they approach the stagnation point. An analytic solution of (8) is not available, but we patch partial solutions together in what is sometimes called the ‘linear-locked’ approximation by noting that near the

upstream boundary  $R$  is close to unity and thus

$$v \frac{\partial R}{\partial y} \approx -R \frac{\partial v}{\partial y}. \quad (19)$$

The deformation is therefore affine and  $R \propto 1/v$ . On the other hand when  $R$  becomes significantly larger than unity, but is still small compared with  $L$ , eqn. (8) can be approximated as

$$v \frac{\partial R}{\partial y} \approx -R \frac{\partial v}{\partial y} - \frac{4}{D}, \quad (20)$$

with solution

$$Rv = -\frac{4y}{D} + \text{constant}. \quad (21)$$

Finally eqn. (21) itself breaks down as  $R$  approaches  $L$  and this value of  $y$  identifies the strand boundary  $y = \delta$ . Patching together an approximate solution at the (arbitrary) choice  $y = \frac{1}{2}$  proves to give good agreement with the numerical solutions of Section 4, except for values of  $D$  close to unity, and is exactly correct in the limit  $D \rightarrow \infty$ . Defining the edge of the strand  $y = \delta$  by where (21) gives  $R = L$  yields

$$-\frac{L\delta}{1 + \Lambda^{1/2}} = \frac{2}{D} - \frac{2 + \Lambda^{1/2}}{2(1 + \Lambda^{1/2})}.$$

Substituting for  $\delta = \Lambda/\hat{c}L^3$  we obtain

$$\Lambda + \hat{c}L^2 \left( \frac{2}{D} - \frac{1}{2} \right) \Lambda^{1/2} + \left( \frac{2}{D} - 1 \right) \hat{c}L^2 = 0. \quad (22)$$

This quadratic equation provides a self-consistent solution for  $\Lambda$  and hence for the strand width  $\delta$ . A number of limiting cases can be recognised.

*Case 1:* If  $\hat{c}L^2 \ll 1$  and  $D > 2$  we obtain

$$\Lambda = \left( 1 - \frac{2}{D} \right) \hat{c}L^2 \quad \text{so that} \quad \delta = \frac{1}{L} \left( 1 - \frac{2}{D} \right). \quad (23)$$

It follows that  $\Lambda$  is small and the flow modification due to the polymers is also small. The result  $\delta \propto 1/L$  was given in ref. [7] on the basis of Newtonian flow kinematics. The result  $\Lambda \propto \hat{c}$  is a consequence of the diluteness of the solution.

*Case 2:* If  $1 \ll \hat{c}L^2 \ll \sqrt{L}$  and  $2 < D < 4$ , we obtain

$$\Lambda = 4 \left( \frac{D-2}{4-D} \right)^2 \quad \text{and} \quad \delta = 4 \left( \frac{D-2}{4-D} \right)^2 \frac{1}{\hat{c}L^3}. \quad (24)$$

For values of  $D$  in this range we predict, perhaps surprisingly, that the strand width falls as the polymer concentration rises. The flow modification is of order unity.

Case 3: If  $1 \ll \hat{c}L^2 \ll \sqrt{L}$  and  $D > 4$ , we obtain

$$\Lambda = \frac{\hat{c}^2 L^4}{4} \left(1 - \frac{4}{D}\right)^2 \quad \text{with} \quad \delta = \frac{\hat{c}L}{4} \left(1 - \frac{4}{D}\right)^2. \tag{25}$$

In this limit we have the possibility of substantial flow modification even though the strand is thin. The result  $\Lambda \propto \hat{c}^2$  is remarkable for a dilute solution: in a genuinely dilute case (Case 1) no such result would be possible; but for a semi-dilute system of rods significant flow modification is permitted within the range of applicability of the theory and, although entanglement effects have been neglected, interactions mediated by the solvent can produce results that are non-linear in  $\hat{c}$ .

Case 4: If  $\hat{c}L^2 \geq \sqrt{L}$  our solution fails, for then variations in the strain rate within the strand become significant.

*Formation of birefringent pipes*

In order to reduce the strain rate sufficiently that the polymers will collapse as they approach the origin it is necessary for the flow modification to be large, and thus only in Case 3 is there a possibility that a pipe will be formed. We may examine this possibility by imposing the requirement that the strain-rate  $U'$  is low enough at  $y = 0$  for the stretch-coil transition to take place. From (5), this requires that

$$\frac{4}{DL} \geq U' = \frac{1}{1 + \Lambda^{1/2}}. \tag{26}$$

In consequence we need  $\Lambda^{1/2} \gg 1$ . Substituting in our result (25) for  $\Lambda$ , we have

$$\hat{c}L > \frac{D^2}{2(D - 4)}. \tag{27}$$

This criterion is shown in the form of a phase diagram in Fig. 5. This analysis predicts the possibility of a pipe for sufficiently large concentrations provided that  $D$  exceeds 4, but is not too large. We note that in the opposed-jet experiment the critical value of  $D$  is rather lower than 4, and no upper limit on  $D$  is seen for pipe formation: it may be, however, that the flare instability occurs before this upper boundary can be reached (see Fig. 2). We see too that only for  $\hat{c} > \hat{c}_+ = 8/L$  is it possible for a pipe to occur.

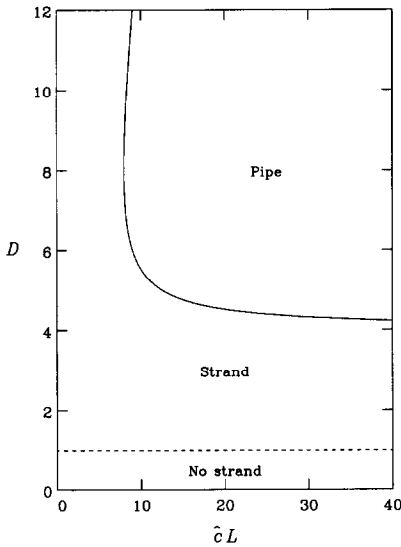


Fig. 5. Phase diagram showing the onset of pipe formation as a function of  $\hat{c}L$  and  $D$ .

A difficulty with our analysis above is that the strands are no longer thin when the pipes are formed. Pipes occur according to eqn. (27) only when  $\hat{c}L = O(1)$  and so eqn. (25) gives that the thickness  $\delta = O(1)$ . As our solution for the flow (14) is based on the assumption that  $\delta \ll 1$ , the criterion (27) must, therefore, be viewed as merely suggestive. A numerical solution for thick strands is needed.

### 3.2. Axisymmetric flow for a thin strand

A similar analysis to the above can be performed for axisymmetric flow. Again the thin strand approximation leads to a criterion that pipes are formed, but only when the strand is thick. Experimental results for the opposed-jet device suggest that birefringent pipes generally occur only in circumstances where the strand occupies a significant proportion of the tube. For this case it is necessary to examine the flow within the strand itself and a numerical solution is needed.

## 4. Thick strands

### 4.1 Planar flow

For Stokes flow outside the strand we have noted that

$$\frac{\partial^2 u}{\partial y^2} = 0 \quad \delta < y < 1.$$

Within the strand (which we assume is uniform in  $x$ —see Section 2.3.3) the high extensional viscosity  $\mu_p$  gives rise to an additional term so that

$$\frac{2\mu_p}{b^2} \frac{\partial^2 u}{\partial x^2} + \frac{\mu}{a^2} \frac{\partial^2 u}{\partial y^2} = 0 \tag{28}$$

In this equation  $\mu_p$  itself depends upon  $y$  because the degree of polymer stretch may vary across the strand, and in particular when a pipe is formed at the centre of the strand  $\mu_p = \mu$  at  $y = 0$ . Fortunately, however, the flow field is remarkably insensitive to the variation of  $\mu_p$  with  $y$  provided that the integrated force exerted by the strand is fixed (see Section 4.4). In consequence we make the further simplifying assumption in solving (28) that  $\mu_p = \bar{\mu}_p$ , a constant across the strand. For convenience we define  $\alpha$  as

$$\alpha = \sqrt{\frac{2\bar{\mu}_p a^2}{\mu b^2}} .$$

The flow within the strand is then given by a normal mode decomposition as

$$\begin{aligned} u(x, y) &= 1 + \frac{\cos(\alpha y) \exp(-x)}{\alpha(1 - \delta) \sin(\alpha\delta) - \cos(\alpha\delta)} \\ &\quad + \sum_{n=0}^{\infty} A_n \cos(\omega_n y) \exp(-\omega_n x/\alpha), \\ v(x, y) &= \frac{1}{\alpha} \left[ \frac{\sin(\alpha y) \exp(-x)}{\alpha(1 - \delta) \sin(\alpha\delta) - \cos(\alpha\delta)} \right. \\ &\quad \left. + \sum_{n=0}^{\infty} A_n \sin(\omega_n y) \exp(-\omega_n x/\alpha) \right], \end{aligned} \tag{29}$$

for  $0 \leq y \leq \delta$ , where  $\omega_n$  is the root of  $\omega \delta \tan(\omega \delta) = \delta/(1 - \delta)$  which lies in the range  $n\pi < \omega_n < (n + 1)\pi$ , and the constants  $A_n$  are chosen to satisfy the boundary condition  $u(0, y) = 0$ . Outside the strand ( $\delta < y < 1$ ) the velocity is given by

$$\begin{aligned} u(x, y) &= U(x) + \frac{y - \delta}{1 - \delta} [\mathcal{U}(x) - U(x)] \\ v(x, y) &= V(x) - U'(x)(y - \delta) - \frac{(y - \delta)^2}{2(1 - \delta)} [\mathcal{U}'(x) - U'(x)]. \end{aligned} \tag{30}$$

where  $[U(x), V(x)]$  is the velocity at  $y = \delta$ .

4.2. Axisymmetric flow

For axisymmetric flow the governing equations become

$$\frac{\partial}{\partial r} \left( r \frac{\partial w}{\partial r} \right) = 0 \quad \delta < r < 1,$$

$$\alpha^2 \frac{\partial^2 w}{\partial z^2} + \frac{1}{r} \frac{\partial}{\partial r} \left( r \frac{\partial w}{\partial r} \right) = 0 \quad 0 < r < \delta, \tag{28}'$$

and

$$\frac{\partial w}{\partial z} + \frac{1}{r} \frac{\partial}{\partial r} (rv) = 0.$$

Within the strand the flow is again given by a normal mode decomposition as

$$v(r, z) = \frac{1}{\alpha} \left[ \frac{J_1(\alpha r) \exp(-z)}{-\alpha \delta \log \delta J_1(\alpha \delta) - J_0(\alpha \delta)} + \sum_{n=0}^{\infty} A_n J_1(\beta_n r) \exp(-\beta_n z / \alpha) \right],$$

$$w(r, z) = 1 + \frac{J_0(\alpha r) \exp(-z)}{-\alpha \delta \log \delta J_1(\alpha \delta) - J_0(\alpha \delta)} + \sum_{n=0}^{\infty} A_n J_0(\beta_n r) \exp(-\beta_n z / \alpha), \tag{29}'$$

where  $J_0(z)$  and  $J_1(z)$  are Bessel functions of the first kind and  $\beta_n$  are the roots of the equation

$$-\beta \delta \log \delta J_1(\beta \delta) = J_0(\beta \delta).$$

The constants  $A_n$  are chosen to satisfy the boundary condition  $w = 0$  on  $z = 0$ . The velocity  $(v, w)$  outside the strand is given by

$$w(r, z) = \mathcal{U}(z) - \frac{\mathcal{U}(z) - \mathcal{W}(z)}{\log \delta} \log r$$

$$v(r, z) = V(z) - \frac{\mathcal{U}'(z)}{2} (r - \delta) + \frac{\mathcal{U}'(z) - \mathcal{W}'(z)}{4 \log \delta} (2r \log r - r - 2\delta \log \delta + \delta), \tag{30}'$$

where  $[V(z), W(z)]$  is the velocity on  $r = \delta$ .

### 4.3 Method of solution

The aim of our calculation, as in the thin strand case, is to determine  $\bar{\mu}_p$  (and hence  $\alpha$ ) and  $\delta$  as functions of  $c$ ,  $L$ ,  $D$  and  $a/b$ . It proves more convenient to fix  $\alpha$ ,  $L$ ,  $D$  and  $a/b$ , then to calculate the corresponding value of  $\delta$  iteratively; and finally to determine  $c$ .

We suppose first that  $\alpha$  and  $\delta$  are given. We then adjust  $\delta$  iteratively for a given value of  $\alpha$  until  $\partial R/\partial y = 0$  at  $y = \delta$ . We may now determine  $R$  and  $\partial u/\partial x$  as functions of  $y$  throughout the strand. The local effective viscosity is given by eqn. (6) as

$$\mu_p(y) = \frac{2\mu c}{D} \frac{f(R)R^2}{\partial u/\partial x}, \tag{31}$$

and self-consistency for the integrated force requires that

$$\alpha^2 = \frac{2a^2}{\mu b^2 \delta} \int_0^\delta \mu_p(y) \, dy. \tag{32}$$

For chosen values of  $\alpha$ ,  $D$  and  $L$  this equation provides a solution for  $\hat{c}$

$$\hat{c} = \left( \frac{\alpha^2 D \delta}{4} \right) \left[ \int_0^\delta \frac{f(R)R^2}{\partial u/\partial x} \, dy \right]^{-1}. \tag{33}$$

For axisymmetric flow we must average  $\mu_p$  over the area of the strand, and then  $\hat{c}$  is given as

$$\hat{c} = \left( \frac{\alpha^2 D \delta^2}{4} \right) \left[ \int_0^\delta \frac{f(R)R^2}{\partial w/\partial z} r \, dr \right]^{-1}, \tag{34}$$

In the limit of high extensibility ( $L \gg 1$ ) with the strain rate exceeding the stretch–coil critical value  $\partial u/\partial x \gg 1/DL$ , the extensional viscosity,  $\mu_p$ , is given by eqn. (7) in which case eqns. (33) and (34) reduce to the simpler form

$$\hat{c} \approx \frac{\alpha^2}{L^3}. \tag{35}$$

### 4.4 Consistency of the flow model

The flow solutions (30) and (30)' in Sections 4.1 and 4.2 assume that  $\mu_p$  has the constant value  $\bar{\mu}_p$  over the cross-section of the strand. We shall find, however, that, with certain combinations of  $c$ ,  $L$  and  $D$ , the dumb-bells are highly extended only in the outer part of the strand and not along

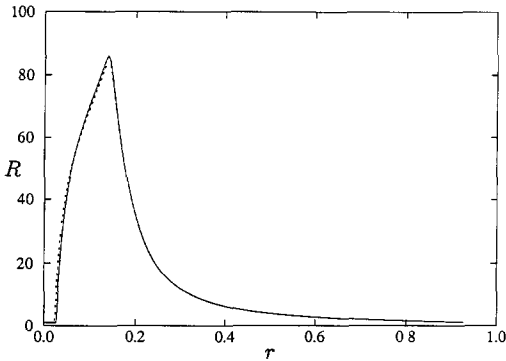


Fig. 6. Comparison between values of  $R$  calculated for  $\hat{c} = 0.2$ ,  $L = 100$  and  $D = 4$  using the two different flow models: (—), constant viscosity model; ( $\cdot \cdot \cdot \cdot$ ), 'pipe' model.

the centre line (i.e. there is a pipe). We have tested the accuracy of our constant strand viscosity approximation by considering an alternative model for axisymmetric flow for which a normal mode structure is available. In this model we take  $\mu_p(r) = \hat{\mu}_p r / \delta$ , so that  $\mu_p$  is equal to zero along the centre line. In Fig. 6 we compare the values of  $R$  calculated with this 'pipe model' and the constant strand viscosity model of Section 4.2 in a case where a pipe is formed. We find that there is little difference in the results. It appears, therefore, that it is the total force exerted on the dumbbells rather than its radial distribution which is important in determining the flow field. This gives us reasonable confidence in our results even for flows where the profiles of  $\mu_p$  are poorly fitted.

#### 4.5. Planar flow: results for thick strands

For concentrations below  $c_+$  (the critical concentration for pipe formation), the polymer remains fully stretched throughout the strand, in which case

$$\alpha^2 = \hat{c}L^3.$$

We can now compare the results of the thick-strand calculations with the asymptotic formulae derived in Section 3 for thin strands. Figure 7 shows the strand width  $\delta$  as a function of  $D$  for values of  $\hat{c}L^2$  of 1, 10, 100 and 300 (with  $L = 100$ ). Formally only the two lowest values of  $\hat{c}L^2$  lie within the range of applicability of the thin-strand theory. Below a Deborah number of approximately 5 the strand width decreases with  $\hat{c}L^2$ , while for Deborah numbers greater than 5, the strand width increases with concentration. This is qualitatively the behaviour predicted from the thin-strand theory where for  $\hat{c}L^2 \gg 1$  the strand width  $\delta$  was found to be proportional

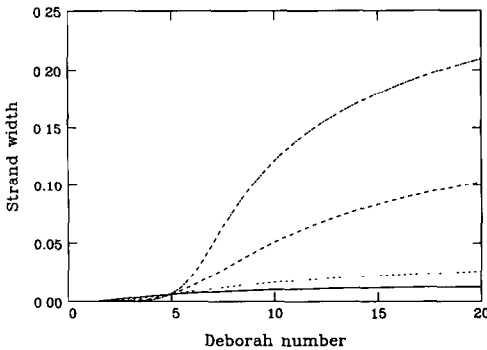


Fig. 7. Strand width as a function of Deborah number for planar flow with  $L = 100$  at various values of  $\hat{c}L^2$ : (—),  $\hat{c}L^2 = 1$ ; ( $\cdot \cdot \cdot \cdot \cdot \cdot$ ),  $\hat{c}L^2 = 10$ ; (— — —),  $\hat{c}L^2 = 100$ ; (— · —),  $\hat{c}L^2 = 300$ .

to  $\hat{c}L^2$  for  $D > 4$ , but proportional to  $(\hat{c}L^2)^{-1}$  for  $D < 4$ . The difference in the value of the critical Deborah number for this transition from 4 to 5 results from the approximation (eqns. (19) and (20)) for the polymer evolution equation (8).

The physical explanation for the two types of behaviour is that the presence of the polymer reduces the strain rate near the strand and a reduction in the strain rate has two opposing effects on the stretching of the polymer. First, the reduction in the strain rate reduces the rate at which the polymers stretch, which reduces the width of the strand. However, the reduction in the strain rate also reduces the magnitude of  $v$  via the continuity equation, and so the polymers move more slowly towards the  $x$ -axis, which tends to increase the strand width. At moderate Deborah numbers the first effect is the more important because the extension rate of the polymer is the difference between  $\partial u / \partial x$  and  $4(R - 1) / DR^2$  and if the strain rate only just exceeds the relaxation rate of the polymer a small change in the strain rate will have a large effect on the strand width. At high Deborah numbers, however, the polymers deform affinely (provided  $R < L$ ) and so  $R \propto -1/v$ . Initially both  $-v$  and  $R$  have values of order unity and so  $\delta$  will be the point at which  $v$  is of order  $-1/L$ . The presence of the strand causes  $v$  to decrease near the strand and so the value of  $\delta$  increases with  $\hat{c}L^2$ .

Figure 8 shows the value of  $\Lambda$  as a function of  $\hat{c}L^2$  for  $L = 100$  and  $L = 10000$  in the limit  $D \rightarrow \infty$ . The values of  $\Lambda$  coincide for the two different values of  $L$  except at large values of  $\hat{c}L^2$ , where the strand width is no longer small. The asymptotic results from eqns. (23) and (25)

$$\Lambda = \hat{c}L^2 \quad \hat{c}L^2 \ll 1$$

$$\Lambda = \frac{1}{4}\hat{c}^2L^4 \quad \hat{c}L^2 \gg 1$$

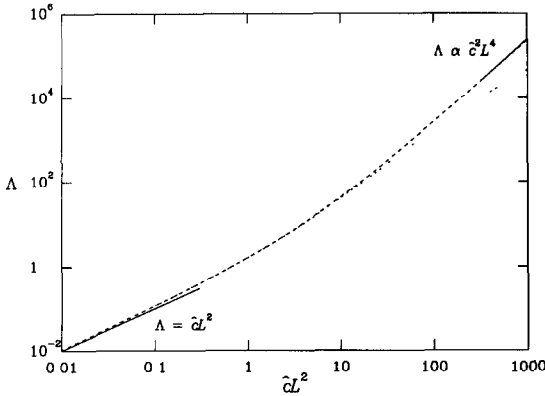


Fig. 8. Plot of  $\Lambda$  as a function of  $\hat{c}L^2$  in the limit  $D \rightarrow \infty$ : ( $\cdot \cdot \cdot \cdot \cdot \cdot$ ),  $L = 100$ ; ( $— — —$ ),  $L = 10000$ .

are shown in this figure and agree with the calculated results for the larger value of  $L$  (though this value is certainly unphysical).

*4.6 Axisymmetric flow: results for thick strands*

Qualitatively, our results for axisymmetric flow are similar to those for planar flow, except that the variation in the strand thickness with concentration is much smaller. This is because the velocity disturbance caused by the strand is proportional to  $\log(1/r)$  rather than  $r$ , and so the flow modification is more localised. Figure 9 shows the variation in the strand radius with Deborah number for the same range of values of  $\hat{c}L^2$  as Fig. 7.

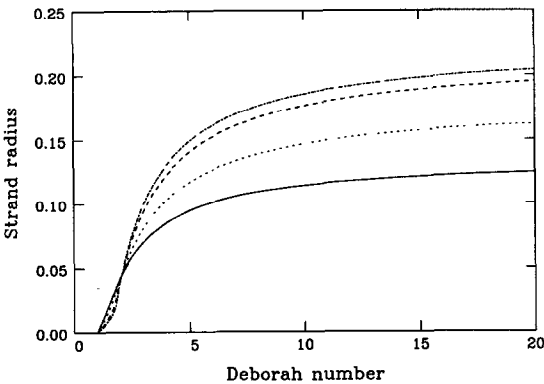


Fig. 9. Strand width as a function of Deborah number for axisymmetric flow with  $L = 100$  at various values of  $\hat{c}L^2$ : ( $—$ ),  $\hat{c}L^2 = 1$ ; ( $\cdot \cdot \cdot \cdot \cdot \cdot$ ),  $\hat{c}L^2 = 10$ ; ( $— — —$ ),  $\hat{c}L^2 = 100$ ; ( $— \cdot —$ ),  $\hat{c}L^2 = 300$ .

Experimental measurements of the width of the birefringent strand have been performed by Müller et al. [11] using the opposed-jet device described in Section 1. They observe an approximately four-fold increase in the width of the birefringent line between a 0.02% and a 0.35% solution of monodisperse polystyrene, which correlates with, but is rather larger than, our calculated increase shown in Fig. 9. On the other hand, in the experiments the strand radius increases with polymer concentration at all flow rates at which strands are observed, whereas in our calculations the strand radius decreases with concentration for Deborah numbers between 1 and 1.8, though there can be difficulties of numerical resolution when the strand width becomes very small. We do not understand this discrepancy.

In the experiments the strand radius initially increases with strain rate, as found in our simulations. However, at higher strain rates the strand width decreases again. We believe that this subsequent decrease is due to inertia (the Reynolds number for these experiments is of the order of 100) as similar experiments with more viscous solvents do not show this behaviour (see Section 7). For very low concentrations the strand radius asymptotes to about  $\frac{1}{6}$ th of the jet radius at high strain rates. The strand width at low concentrations and high Deborah numbers is approximately  $a/\sqrt{L}$  (if the polymer deforms affinely  $R \propto -1/rv$  and so for  $v = -r/2$  this gives  $\delta^* = a/\sqrt{L}$ ) which suggests that an approximate value for  $L$  is 36.

Cathey and Fuller [14] have also measured the width of the birefringent strand using similar experimental apparatus to that used by Müller et al. [11]. The solvents used in these experiments were more viscous than those used by Müller and the strand width is observed to increase with strain rate towards a finite limit with no subsequent decrease.

## 5. Birefringent pipes

The analytical thin-strand model of Section 3 is able to suggest that pipes may form but becomes inconsistent once the pipe has formed. The numerical finite strand width model, however, allows us to investigate the structure of the pipe.

### 5.1 Planar flow

Figure 10 shows the phase diagram for the onset of a pipe as a function of  $\hat{c}$  and  $D$  for  $L = 100$  from the numerical calculations for a strand of finite width. Comparing this with Fig. 5, the phase diagram for the thin-strand model, we see that the dependence of pipe formation on concentration and Deborah number is approximately the same.

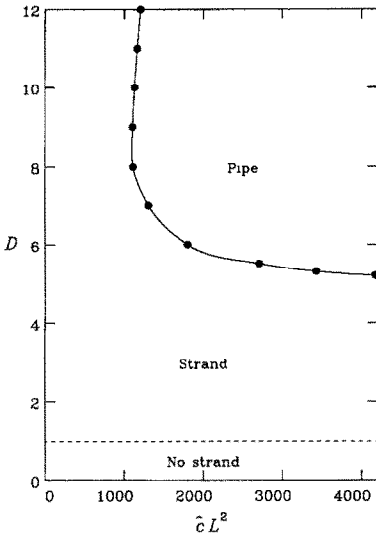


Fig. 10. Phase diagram of the formation of a pipe in planar flow as a function of  $\hat{c}L^2$  and  $D$  with  $L = 100$ .

Pipes do not occur below a critical concentration,  $\hat{c}_+$ . The thin-strand model predicted this to be  $8/L$  (from eqn. (27)) and at this value a pipe will form at  $D = 8$ . In Fig. 10 we see that for  $L = 100$  the value of  $\hat{c}_+$  is approximately 0.11 (slightly larger than the estimate of 0.08), and the corresponding value of  $D$  is approximately equal to 8.

Even at concentrations above  $\hat{c}_+$  pipes do not form for Deborah numbers less than about 5. In the thin-strand analysis we found for  $D < 4$  that the strand width decreased with  $\hat{c}$  and that  $\Lambda$  was always of order unity. The formation of a pipe requires a large value of  $\Lambda$ . At Deborah numbers above 8 the minimum concentration required to form a pipe increases with  $D$  because a larger value of  $\Lambda$  is required to produce the necessary reduction in strain rate.

Although pipes are seen in planar flows (e.g. by Cressely et al. [15,16]) there are no quantitative measurements with which to compare our results. For this reason we concentrate on axisymmetric flow where we can compare our results with observations from suction-jet experiments [8–13].

## 5.2 Axisymmetric flow

Figures 11 and 12 show phase diagrams for pipe formation in axisymmetric flow for  $L = 36$  and  $L = 100$  respectively. Changing the value of  $L$  has

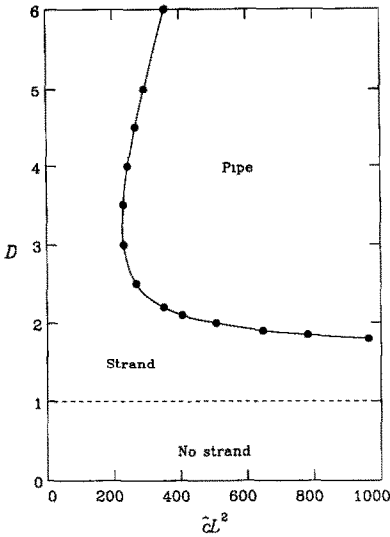


Fig. 11. Phase diagram of the formation of a pipe in axisymmetric flow as a function of  $\hat{c}L^2$  and  $D$  with  $L = 36$ .

little effect on the form of the phase diagram apart from changing the scale of the concentration dependence. The phase diagram for axisymmetric flow has approximately the same form as that for planar flow except that the

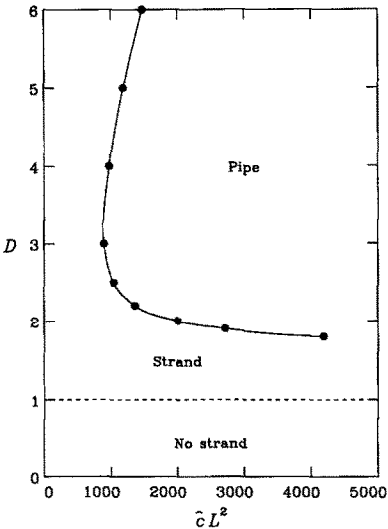


Fig. 12. Phase diagram of the formation of a pipe in axisymmetric flow as a function of  $\hat{c}L^2$  and  $D$  with  $L = 100$ .

minimum Deborah number required to form a pipe is smaller (approximately 1.8 compared to 5 for planar flow).

Comparing Figs. 11 and 12 with the experimental phase diagram for monodisperse poly(styrene) from Keller et al. [9] in Fig. 2, we see that the shape of the lower branch of the strand–pipe transition is essentially the same. In both the experiments and theory there is a critical concentration  $\hat{c}_+$  below which pipes are not found at any Deborah number. At concentrations,  $\hat{c}$ , above  $\hat{c}_+$  pipes are observed only at Deborah numbers greater than a critical value that depends strongly on  $\hat{c}$ . For Deborah numbers below this critical value but greater than unity a thin strand is present, but its thickness is too small to produce a sufficiently large modification to the flow. The predicted value of the critical Deborah number is somewhat greater than the experimental value. The difference between the experimental and theoretical phase diagrams at large  $D$  may be entirely due to the flare instability which we have not studied.

The slight decrease with concentration seen in Fig. 2 for the coil–stretch transition may result from the small increase in the shear viscosity of the solution due to the addition of polymer. This effect is easily incorporated in the analysis but is neglected for the dilute theory presented here.

### 5.3 The structure of the pipe

Figures 13(a)–13(b) show the dumbbell extension,  $R$ , as a function of radius for two different concentrations ( $\hat{c}L^2 = 130$  and  $\hat{c}L^2 = 390$  respectively) at a Deborah number of 4. A pipe is formed only for the higher concentration. The dashed curve on each graph shows the extension rate,  $\partial w/\partial z$ , as a function of  $r$  and the horizontal dotted line indicates the critical extension rate for the stretch–coil transition. In Fig. 13(a) the extension rate always remains above the critical level and so, although the dumbbells do decrease in length within the strand, they ultimately attain an equilibrium length on the upper solution branch of the hysteresis curve (see Fig. 4). In Fig. 13(b) the extension rate falls below the stretch–coil transition value in the centre of the strand and so the dumbbells collapse forming a pipe. Note that there is only a small variation in the extension rate within the strand (as assumed in the thin-strand approximation).

As the dumbbells reduce in length, their rate of collapse (which is proportional to  $1/R$ ) increases. Also, the velocity of the dumbbells towards the axis decreases, and so the final stage of collapse occurs rapidly in space. This produces a sharp interface between the regions of extended and unextended dumbbells, as is observed experimentally where there is an abrupt change between birefringent and non-birefringent regions of the flow.

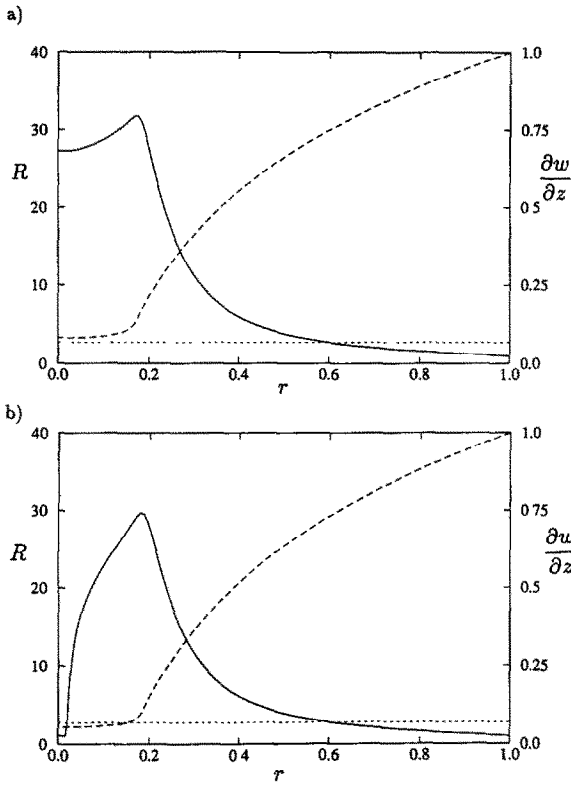


Fig. 13. Dumbbell extension,  $R$ , (—) and strain rate,  $\partial w/\partial z$ , (---) for  $L = 36$  and  $D = 4$  at concentration: (a)  $\hat{c}L^2 = 130$ ; (b)  $\hat{c}L^2 = 390$ . Dotted lines indicates critical strain rate for stretch-coil transition.

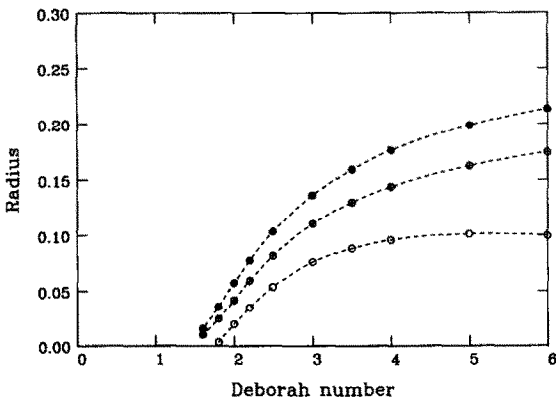


Fig. 14. The structure of the birefringent strand in axisymmetric flow as a function of Deborah number, for  $L = 100$  and  $\hat{c} = 0.5$ : (●), outer radius at which  $R = L/2$ ; (○), inner radius at which  $R = L/2$ ; ⊕ strand radius ( $\delta$ ).

The variation of the flow birefringence with increasing Deborah number is shown in Fig. 14. Here, we have chosen (somewhat arbitrarily) to define the region of birefringence to be where the dumbbells are extended to at least half of their maximum possible length (i.e.  $R \geq \frac{1}{2}L$ ). In this figure the open and closed circles are respectively the inner and outer radii of the birefringent region. The intermediate points (denoted by circles with a central cross) are the positions of the strand radius  $\delta$  (defined to be where the extension is greatest).

Above a Deborah number of unity a very thin birefringent strand appears. The width of this strand increases with Deborah number until at about  $D = 1.8$  a pipe is formed. Both the outer and inner pipe radii expand with increasing Deborah number up to around 5, when the inner radius begins to contract. Apart from the final stage, this sequence corresponds directly to the observations of Keller et al. [9]. The reason why the contraction of the inner radius of the pipe is not seen in the experiment may be that the flow is unstable at these Deborah numbers.

#### 5.4 Other birefringent structures

With the simplified models introduced in Section 2 we have been able to reproduce the birefringent pipe structure and to explain the form of the phase diagram for the strand–pipe transition. However, we do not see the other more complex structures which are also observed in experiments. For example, in order for a second birefringent line to appear the extension rate near the centre line must increase again after it has dropped below the stretch–coil transition value. This cannot happen in our model as the extension rate will always decrease with decreasing distance from the centre line  $x = 0$ , owing to the absence of a pressure gradient. It should be noted that the second line appears only when the pipe radius is comparable with the radius of the jet, and so the lubrication approximation made in deriving the flow model is no longer valid. A more sophisticated flow model is needed which takes account of this and of the more complex polymer stress distribution.

The flare instability has also not been investigated. The pipe–flare interface shown in Fig. 2 roughly follows a line of constant  $\Lambda$ . This suggests that the instability may arise from the modification of the flow by the birefringent strand, but this requires further investigation. One method of testing this hypothesis would be to compare the phase diagrams for polymers of different molecular weights (i.e. different values of  $L$ ). If the flare instability is caused by flow modification then it should occur at the same value of  $\Lambda$  for different  $L$ , whereas the values of  $\Lambda$  necessary to produce the pipe increase with increasing molecular weight.

### 6. FENE dumbbells with linear friction

The polymer model of previous sections incorporates non-linear friction (or hydrodynamic drag). FENE dumbbell models with linear friction are easier to handle numerically (see e.g. ref. [5]). Do they also produce pipes?

With linear friction, (5) is replaced by

$$\frac{dR}{dt} = ER - \frac{f(R)}{D}(R - 1), \tag{36}$$

but the additional stress exerted by the dumbbells is unchanged.

There are two important differences in the resulting rheology. First, in steady extension at high Deborah numbers the polymer stress is proportional to  $L^2$  and not  $L^3$ . This consequently reduces the degree of flow modification. Second, there is no hysteresis between the coil–stretch and stretch–coil transitions, and so the strain-rate need be reduced only by a factor of  $1/D$  (rather than  $1/DL$ ) to generate a pipe.

For planar flow we can use the thin-strand model of Section 3 to determine the values of the parameters  $\hat{c}$ ,  $L$  and  $D$  that lead to pipe formation. The velocity along the incoming stagnation streamline is still given by eqn. (18) as

$$v = \frac{1}{1 + \Lambda^{1/2}}y - \frac{\Lambda^{1/2}}{2(1 + \Lambda^{1/2})}y^2,$$

provided that  $\Lambda^{1/2}\delta \ll 1$ , but now  $\Lambda$  is equal to  $\hat{c}L^2\delta$  and not  $\hat{c}L^3\delta$ .

For large values of  $D$  and  $L$  the degree of stretching of the polymer along this streamline can be calculated. For small values of  $R$  the polymer deforms affinely and  $R \propto 1/v$ , while for  $1 \ll R \ll L$  eqn. (36) can be approximated as

$$v \frac{\partial R}{\partial y} = -R \frac{\partial v}{\partial y} - \frac{R}{D}. \tag{37}$$

Once again we match these two approximations at  $y = \frac{1}{2}$ , and then by imposing the condition that  $R = L$  at  $y = \delta$  we obtain

$$\frac{L\delta(2 + \Lambda^{1/2}\delta)}{(2 + \Lambda^{1/2})} = \left[ \frac{\delta(\Lambda^{1/2} + 4)}{2 + \delta\Lambda^{1/2}} \right]^{(1 + \Lambda^{1/2})/D}, \tag{38}$$

with  $\Lambda = \hat{c}L^2\delta$ . In order for a pipe to form, the strain rate at the origin must be below the critical strain rate for the stretch–coil transition, (i.e.  $U' < 1/D$  at  $y = 0$ ). This requires that

$$\Lambda^{1/2} + 1 > D, \tag{39}$$

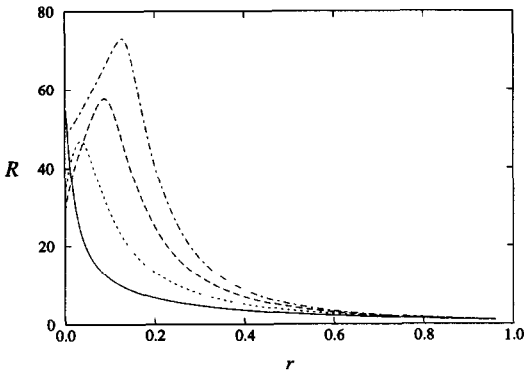


Fig. 15. Dumbbell length,  $R$  as a function of radius for the linear friction model in axisymmetric flow with  $\hat{c} = 0.5$  and  $L = 100$ , at various values of  $D$ : (—),  $D = 1.5$ ; ( $\cdot \cdot \cdot \cdot \cdot$ ),  $D = 3$ ; (---),  $D = 6$ ; (- · -),  $D = 12$ .

with equality when a pipe is just formed. At this point eqn. (38) gives

$$L(2 + \Lambda^{1/2}\delta)^2 = (\Lambda^{1/2} + 4)(\Lambda^{1/2} + 2). \quad (40)$$

Since  $L \gg 1$  (with  $\Lambda^{1/2}\delta \ll 1$ )

$$\Lambda \approx 4L \quad \text{so} \quad D \approx 2L^{1/2} \quad \text{with} \quad \delta \approx \frac{4}{\hat{c}L}. \quad (41)$$

Thus pipes occur only at Deborah numbers higher than  $2\sqrt{L}$  and since  $\Lambda^{1/2}\delta \ll 1$  we require additionally that  $\hat{c}\sqrt{L} \gg 1$ . Solving eqns. (39) and (40) numerically, we find that for  $\hat{c} < 1$  pipes occur only for  $L \geq 3000$  and  $D \geq 140$ . Such high values of  $D$  are well beyond the range of the suction-jet experiments.

Figure 15 shows the dumbbell length,  $R$ , as a function of radial distance in axisymmetric flow at various values of  $D$  for  $\hat{c} = 0.5$  and  $L = 100$ . These results were calculated using the method described in Section 4. Even at this high concentration a pipe is not seen at any value of  $D$ .

These results show that pipes of the kind found earlier do not occur for dilute concentrations of dumbbells with linear friction at experimentally achievable Deborah numbers. This is because the linear dumbbells are unable to affect the flow when the local strain rate drops below the coil–stretch transition: linear dumbbells do not have the hysteresis seen in Fig. 4. Thus although the linear friction model does produce a birefringent strand [4] it cannot reproduce the birefringent pipe.

This calculation shows that this strongly non-Newtonian flow can provide a subtle discrimination between models. As already noted [6] many models (e.g. Giesekus, Phan–Thien–Tanner) with high Trouton ratios will produce

birefringent strands; however, only a smaller class produce birefringent pipes at plausible parameter values.

## 7. The effect of inertia

The calculations in the previous sections neglected fluid inertia. In many of the experiments the Reynolds numbers ( $Re = \rho U_{\infty} b / \mu$ ) are quite large (typically of the order of 100). However, there is little qualitative difference between the birefringence behaviour of these experiments and others with more viscous solvents for which the Reynolds numbers are small. There is, however, a difference in the behaviour of the strand width at high strain rates. In both our results and the low Reynolds number experiments of Cathey and Fuller [14] the strand width increases monotonically towards a finite limit. On the other hand, Müller et al. [11] (who used low viscosity solutions, for which  $Re$  is of the order of 100) observe that the strand width increases with strain rate at low strain rates but then decreases again at higher strain rates. In this section we show that inertia is responsible for this decrease in strand width.

At high Reynolds number,  $Re$ , an inertial boundary layer is generated at the margin of the birefringent strand. Moving radially outward from the axis there are now three different regions of flow.

(1) The birefringent strand where the polymer molecules are highly extended and the extensional viscosity of the solution is high.

(2) The inertial boundary layer; a region outside the strand of thickness of order  $1/\sqrt{Re}$  where the effect of the polymer can be neglected, but the fluid viscosity is important.

(3) The outer region, where both non-Newtonian stresses and viscosity can be neglected. In this region we have a potential flow and for small values of  $z$  the fluid velocity is given by

$$v = -\frac{1}{2}r, \quad w = z.$$

### 7.1 The birefringent strand

Within the strand the fluid inertia is negligible (see below) so the momentum equation remains (eqn. (8))

$$\alpha^2 \frac{\partial^2 w}{\partial z^2} + \frac{1}{r} \frac{\partial}{\partial r} \left( r \frac{\partial w}{\partial r} \right) = 0.$$

Provided that the strand thickness is small,  $w$  is approximately uniform

across the strand and across the strand we obtain

$$r \frac{\partial w}{\partial r} \approx - \frac{\alpha^2 \delta^2}{2} \frac{\partial^2 w}{\partial z^2} \quad \text{at } r = \delta. \tag{42}$$

Near the stagnation point  $w$  is approximately linear in  $z$ , so that

$$w \approx Ez,$$

for some unknown strain rate  $E$ . The length scale for variations in the  $z$ -direction is  $1/E$ , and so for small values of  $z$

$$\frac{\partial^2 w}{\partial z^2} \approx E^3 z,$$

arbitrarily assigning the multiplicative constant to unity. With these approximations, the boundary conditions at  $r = \delta$  for the inertial boundary layer calculation are

$$\frac{\partial w}{\partial r} = \frac{\alpha^2 E^3 \delta}{2} z, \quad w = Ez \quad \text{and by continuity} \quad v = -\frac{1}{2}Er. \tag{43}$$

Finally we note that fluid inertia is negligible compared to the extensional stress gradient in the strand provided that

$$\left| Re w \frac{\partial w}{\partial z} \right| \ll \left| \alpha^2 \frac{\partial^2 w}{\partial z^2} \right|. \tag{44}$$

Substituting our expressions for  $w$  and  $\partial^2 w / \partial z^2$  from eqn. (43), this requires that

$$\alpha^2 \gg \frac{Re}{E},$$

which is satisfied for sufficiently large values of  $\alpha$ .

### 7.2 The inertial boundary layer

To obtain the flow within this boundary layer we adapt the solution of Hiemenz (see, for example, Ref. 21) for flow near a stagnation point on a rigid boundary. Outside the strand the fluid is Newtonian and so in dimensionless variables the vorticity ( $\boldsymbol{\omega} = \nabla \wedge \mathbf{u}$ ) satisfies

$$\frac{\partial \boldsymbol{\omega}}{\partial t} + \mathbf{u} \cdot \nabla \boldsymbol{\omega} = \boldsymbol{\omega} \cdot \nabla \mathbf{u} + \frac{1}{Re} \nabla^2 \boldsymbol{\omega}. \tag{45}$$

For steady axisymmetric flow with velocity  $(v, w)$  and vorticity  $\omega$  this equation becomes

$$v \frac{\partial \omega}{\partial r} + w \frac{\partial \omega}{\partial z} = \frac{\omega v}{r} + \frac{1}{Re} \left[ \frac{\partial^2 \omega}{\partial z^2} + \frac{1}{r} \frac{\partial}{\partial r} \left( r \frac{\partial \omega}{\partial r} \right) - \frac{\omega}{r^2} \right]. \tag{46}$$

For small values of  $z$ ,  $w$  is proportional to  $z$  and so we seek a solution to eqn. (46) of the form

$$\mathbf{u} = \left( -\frac{f(r)}{r}, \frac{zf'(r)}{r} \right), \quad \omega = -\frac{z}{r} \left( \frac{f'(r)}{r} \right)',$$

for some function  $f(r)$  to be determined. The vorticity equation (46) gives

$$\left( \frac{f'}{r} \right)^2 - \frac{f}{r} \left( \frac{f'}{r} \right)' - \frac{1}{rRe} \left[ r \left( \frac{f'}{r} \right)' \right]' = 1, \tag{47}$$

which is the axisymmetric analogue of the Hiemenz equation. At the strand boundary both the velocity and the shear rate are continuous, and so the boundary conditions on  $f(r)$  are (from eqn. (43))

$$f(\delta) = \frac{1}{2}E\delta^2, \quad f'(\delta) = E\delta, \quad f''(\delta) = E + \frac{\alpha^2 E^3 \delta^2}{2} \tag{48}$$

and  $f \approx \frac{1}{2}r^2$  for  $r \gg \frac{1}{\sqrt{Re}}$ .

This equation can be solved numerically by a shooting technique to find the unknown parameter  $E$ .

### 7.3 Calculating the strand width

In the high Deborah number limit the dumbbells deform affinely for  $R < L$  and therefore  $R$  is inversely proportional to  $rv$  (see Section 4.6). Since the dumbbells are fully extended at  $r = \delta$ ,  $\delta$  must satisfy

$$\delta = \sqrt{\frac{1}{LE}}, \tag{49}$$

The value of  $\delta$  in the boundary layer calculation is then varied until it satisfies eqn. (49).

### 7.4 Numerical results

The variation in the strand width with Reynolds number for various values of  $\alpha$  is shown in Fig. 16. The strand width decreases with Reynolds number towards a value of  $1/\sqrt{L}$ . This occurs because the strand affects the flow only within the inertial boundary layer. In the outer region the polymers behave exactly as they would in a very dilute solution where there is no flow modification. As the Reynolds number increases, the inertial boundary layer reduces in thickness and so the strand width tends towards

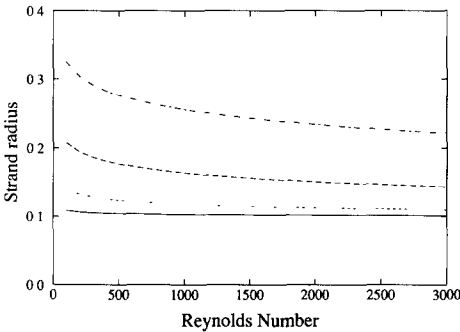


Fig. 16. Strand width as a function of Reynolds number for  $L = 100$  at various values of  $\hat{c}L^2$ : (—),  $\hat{c}L^2 = 1$ ; ( $\cdot \cdot \cdot \cdot \cdot \cdot$ ),  $\hat{c}L^2 = 10$ ; (— — —),  $\hat{c}L^2 = 100$ ; (—  $\cdot$  —),  $\hat{c}L^2 = 1000$ .

its value in the limit of zero concentration. This variation is observed in the birefringence experiments of Müller et al. [9]. At a strain rate of  $6000 \text{ s}^{-1}$  the strand width is approximately  $100 \mu\text{m}$  for a concentration of 0.02% and approximately  $300 \mu\text{m}$  for a concentration of 0.125%. When the strain rate is increased to about  $24000 \text{ s}^{-1}$  the strand widths at these concentrations are respectively about  $70 \mu\text{m}$  and  $100 \mu\text{m}$ . Thus the strand widths decrease with strain rate and the difference between the strand widths at different concentrations is much smaller at higher strain rates.

## 8. Conclusions

We have examined the steady flow of a dilute polymer solution near a stagnation point. In the limit of large extensibility  $L$ , the polymer is highly extended only within a narrow strand of width  $\delta$ . By considering a simplified model of the flow outside the strand, analytic expressions for  $\delta$  (and hence for  $\lambda$ ) can be obtained in terms of the fundamental parameters  $\hat{c}$ ,  $L$  and  $D$ .

For values of  $\hat{c}L$  greater than 8 we find a range of Deborah numbers for which the extension rate within the strand is less than the stretch-coil transition value and so the polymers collapse back to their coiled state. This provides a mechanism for the formation of birefringent pipes observed in suction-jet experiments.

The predicted variation in birefringence behaviour obtained from these models is in good agreement with phase diagrams obtained from experimental observations by Keller et al. [9]. This enables us to explain the observed variation in the birefringence behaviour with concentration and extension rate. Our results also demonstrate that pipes can occur in dilute solutions without the need for entanglements between polymer molecules.

However, interactions mediated by the solvent are crucial to the production of a large polymeric stress.

The deformation of a polymer molecule is here modelled as the extension of an elastic dumbbell incorporating both a non-linear spring and non-linear hydrodynamic drag. We show that the results cannot be reproduced using a simpler dumbbell model with linear friction, as it is not possible to obtain the required degree of flow modification. The effectiveness of other models having a high but finite extensional viscosity at producing a pipe phenomenon has yet to be established.

Further work is needed to examine the variation of the stretch of the polymers along the length of the strand, and to examine the onset of instabilities.

## References

- 1 T. Sridhar, *J. Non-Newtonian Fluid Mech.*, 35 (1990) 85–92.
- 2 G.K. Batchelor, *J. Fluid Mech.*, 44 (1971) 419–440.
- 3 D.G. Crowley, F.C. Frank, M.R. Mackley and R.C. Stephenson, *J. Polym. Sci.*, A2, 14 (1976) 1111–1119.
- 4 O.G. Harlen, J.M. Rallison and M.D. Chilcott, *J. Non-Newtonian Fluid Mech.*, 34 (1990) 319–349.
- 5 M.D. Chilcott and J.M. Rallison, *J. Non-Newtonian Fluid Mech.*, 29 (1988) 381–432.
- 6 O.G. Harlen, *J. Non-Newtonian Fluid Mech.*, 37 (1990) 157–173.
- 7 J.M. Rallison and E.J. Hinch, *J. Non-Newtonian Fluid Mech.*, 29 (1988) 37–55.
- 8 A. Keller and J.A. Odell, *Colloid Polym. Sci.*, 263 (1985) 181–201.
- 9 A. Keller, A.J. Müller and J.A. Odell, *Progr. Colloid Polym. Sci.*, 75 (1987) 179–200.
- 10 A. Chow, A. Keller, A.J. Müller and J.A. Odell, *Macromolecules*, 21 (1988) 250–256.
- 11 A.J. Müller, J.A. Odell and A. Keller, *J. Non-Newtonian Fluid Mech.*, 30 (1988) 99–118.
- 12 J.A. Odell, A.J. Müller and A. Keller, *Polymer*, 29 (1988) 1179–1190.
- 13 A.J. Müller, J.A. Odell and J.P. Tatham, *J. Non-Newtonian Fluid Mech.*, 35 (1990) 231–250.
- 14 C.A. Cathey and G.G. Fuller, *J. Non-Newtonian Fluid Mech.*, 34 (1990) 63–88.
- 15 R. Cressely, R. Hocquart and O. Scrivener, *Optica Acta*, 25 (1978) 559–571.
- 16 R. Cressely, R. Hocquart and O. Scrivener, *Optica Acta*, 26 (1979) 1173–1181.
- 17 K. Gardner, E.R. Pike, M.J. Miles, A. Keller and K. Tanaka, *Polymer*, 23 (1982) 1435–1442.
- 18 E.J. Hinch, *Polymères et Lubrification, Colloques Internationaux du C.N.R.S.*, 233 (1974) 241–247.
- 19 J.A. Odell, personal communication.
- 20 Y. Rabin, F.S. Henyey and D.B. Creamer, *J. Chem. Phys.*, 85 (1986) 4696–4701.
- 21 G.K. Batchelor, *An Introduction to Fluid Dynamics*, Cambridge University Press, 1967.

## Appendix: Variation of strand width with distance from the stagnation point

In the body of the text and in refs. [4] and [6] we have assumed that the width,  $\delta$ , of the birefringent strand produced by an isolated stagnation

point is uniform in  $x$ . This is consistent with both birefringence observations [8–13] and the numerical solutions of Chilcott and Rallison [5]. In this Appendix we prove that this assumption is valid asymptotically in the limit of small  $\delta$  at points along the strand where the local extension rate is large compared to the stretch–coil transition value. The proof given here is valid for thin strands that can produce large flow modifications. Unfortunately, as noted in Section 2.3, the generation of pipes requires *very* large flow modification that falls outside the formal range of validity of this proof.

For simplicity, we consider planar flow with a straight strand. The extension of this proof to a curved strand (see e.g. ref. [4]) is straightforward, provided that the radius of curvature of the strand is large compared to the strand width, and the necessary modifications are indicated at the end of this Appendix. The same procedure may be used for axisymmetric flow.

In order to become highly extended a polymer molecule must reside within the flow for a time of order  $\log L$ , and for large values of  $L$  (with  $\hat{c}L \ll 1$ ) it must pass close to the stagnation point. Therefore, throughout its history it remains close to either the incoming stagnation streamline or the birefringent strand. By forming asymptotic expressions for the fluid velocity in the region near the incoming streamline and in the region near the birefringent strand, we shall show that the distance from the downstream stagnation streamline at which the polymers become fully extended is independent of the distance from the stagnation point.

Consider a planar flow with a stagnation point at the origin. Cartesian coordinates are defined such that the birefringent strand lies along the  $x$ -axis, with the incoming stagnation streamline along the  $y$ -axis (see Fig.

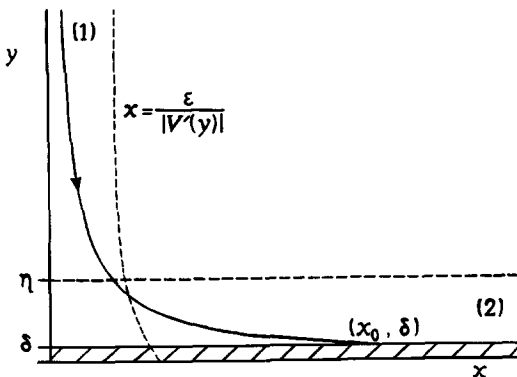


Fig. 17. Sketch showing the path of a polymer molecule which intersects the strand, and regions (1) and (2).

17). For convenience we use the dimensionless variables defined in Section 2.

*Region (1): small x*

For suitably small values of  $x$  the velocity component in the  $y$ -direction is approximately independent of  $x$  so the velocity,  $\mathbf{u} = (u, v)$  is given by

$$u \approx -xV'(y), \quad v \approx V(y), \tag{A1}$$

where  $V(y)$  is the velocity along the  $y$ -axis. For small values of  $\Lambda$  the length scale of the flow in the  $x$ -direction is equal to unity and so this approximation is valid for the region  $x < \epsilon$  where  $\epsilon \ll 1$  is a constant to be determined. For large values of  $\Lambda$ , the presence of the strand reduces the extension rate near the  $x$ -axis (the extension rate along the strand will be of order  $\Lambda^{-1/2}$ ). This increases the length scale of the flow (to  $\Lambda^{1/2}$  along the strand) and so increases the range of values of  $x$  for which the approximation is valid. The  $x$  length scale will be approximately inversely proportional to the extension rate,  $-V'(y)$ , and so in general eqn. (A1) is valid in the region

$$x > 0, \quad y > 0, \quad x < \frac{\epsilon}{|V'(y)|}, \quad \text{with } \epsilon \ll 1. \tag{A2}$$

*Region (2): small y*

In the region close to the strand,  $u$  is approximately independent of  $y$ , and so for small values of  $y$  the velocity is given by

$$u \approx U(x), \quad v \approx -yU'(x), \tag{A3}$$

where  $U(x)$  is the velocity along the  $x$ -axis. If  $\Lambda$  is small, the  $y$  length scale of the flow is equal to unity, and so this approximation is valid in the region  $y < \eta$  for some constant  $\eta$ , with  $\eta \ll 1$ . If  $\Lambda$  is large the extension rate along the strand is smaller than that of the outer flow, producing a shear rate near the strand of magnitude unity for  $1 < x < \Lambda^{1/2}$  and so for small values of  $y$

$$u \approx U(x) + \gamma y \approx xU'(0) + \gamma y \quad 1 < x < \Lambda^{1/2},$$

where  $\gamma$  is of magnitude unity. Therefore the approximation in eqn. (A3) is valid only for  $y \ll U'(0)$ , i.e. within the region

$$x > 0, \quad y > 0, \quad y < \eta, \quad \text{with } \eta \ll U'(0). \tag{A4}$$

*The path of the polymer*

We now show that the path taken by a polymer which becomes fully extended at the point  $(x_0, \delta)$  is confined throughout its history within the union of regions (1) and (2) and that suitably small choices of  $\eta$  and  $\epsilon$  can be made. Provided  $\delta$  is small compared to  $U'(0)$ , we can choose  $\eta$  to be large compared with  $\delta$  so that the strand lies within region (2).

Following the path of the polymer backwards in time, its position  $(x, y)$  satisfies

$$\frac{dy}{dx} = \frac{v}{u} = \frac{-yU'(x)}{U(x)}$$

provided that it remains within region (2), and so

$$y = \frac{\delta U(x_0)}{U(x)}. \quad (\text{A5})$$

This path intersects the boundary of region (1) at the point  $(x_1 = \epsilon/|V'(0)|, y_1)$ , (i.e. at the point where  $U(x) \approx -xV'(0) = \epsilon$ ). Within region (1),  $x$  is inversely proportional to  $-V(y)$  and so the position of the polymer is given by

$$x = \frac{\epsilon y_1}{-V(y)}, \quad (\text{A6})$$

and provided that

$$\left| \frac{V(y)}{y_1 V'(y)} \right| > 1 \quad \text{for } y > y_1 \quad (\text{A7})$$

the path of the polymer will have been entirely within region (1) prior to reaching the position  $(x_1, y_1)$ . Near the strand  $V(y)$  is linear and so (A7) is satisfied. Furthermore, for  $y$  of order unity both  $V(y)$  and  $V'(y)$  will be also of order unity, and so the condition (A7) holds because  $y_1$  is small.

Hence, the path of the polymer lies entirely within the union of regions (1) and (2) if

$$\epsilon \eta > \delta U_m, \quad \text{with } \epsilon \ll 1, \eta \ll U'(0), \quad (\text{A8})$$

where  $U_m$  is the maximum value of  $U(x)$ . In the worst case  $U_m$  is of order unity, and hence provided  $U'(0) \gg \delta$ , we can choose  $\epsilon = 2\sqrt{\delta/U'(0)}$ ,  $\eta = \sqrt{\delta U'(0)}$ . In the extreme case when  $\delta \geq O(U'(0))$ , the  $x$  length scale along the strand will be of order  $1/U'(0) \gg 1$  and so for  $x < \Lambda^{1/2}$  the strand lies within region (1).

### Polymer extension

We now calculate the polymer extension along this path. Within region (1), both  $\partial u/\partial x$  (equal to  $-V'(y)$ ) and  $v$  are independent of  $x$ . Further  $R = 1$  at  $y = 1$  independent of  $x$ . Hence, the extension,  $R$ , of a polymer molecule in this region will be independent of  $x$ .

In region (2), we consider first the high Deborah number limit. If the polymer is assumed to deform affinely, then the extension,  $R$ , satisfies

$$\mathbf{u} \cdot \nabla R = R \frac{\partial u}{\partial x} + O(1/D), \quad (\text{A9})$$

and so from eqn. (A3)

$$\mathbf{u} \cdot \nabla R = RU'(x). \quad (\text{A10})$$

The  $y$  coordinate of the position of the polymer satisfies

$$\frac{dy}{dt} = v = -yU'(x), \quad (\text{A11})$$

and on any trajectory we find that  $R$  is inversely proportional to  $y$  within this region. In the intersection of regions (1) and (2) we have shown that  $R$  is independent of  $x$ , and so the constant of proportionality on all paths is the same. Therefore,  $R$  is independent of  $x$  on all paths which intersect the strand, and so in the high Deborah number limit  $\delta$  is asymptotically constant.

At moderate Deborah numbers there is an additional term in eqn. (A10) arising from the elastic restoring force (see eqn. (5)). The magnitude of this term, relative to the extension of the polymer by the flow, is of order  $1/DRU'(x)$ , and so the above result remains valid provided  $DRU'(x) \gg 1$  in region (2). In this region  $R$  is inversely proportional to  $y$ , and it suffices to impose the additional constraint that  $\eta \ll DLU'(x)\delta$ . Thus the strand width will be asymptotically constant provided that  $U'(x) \gg 1/DL$ .

The analysis above can be generalised to flows where either the strand or the incoming stagnation streamline are curved, by replacing by Cartesian coordinates  $(x, y)$  with streamline coordinates. The approximations within regions (1) and (2) remain valid provided that the widths of these regions are small in comparison to the radius of curvature of the streamlines.